Catalysis Today 153 (2010) 136–142

Contents lists available at ScienceDirect

Catalysis Today

journal homepage: www.elsevier.com/locate/cattod

Three-dimensionally ordered macroporous $LaCo_xFe_{1-x}O_3$ perovskite-type complex oxide catalysts for diesel soot combustion

Junfeng Xu, Jian Liu*, Zhen Zhao**, Jianxiong Zheng, Guizhen Zhang, Aijun Duan, Guiyuan Jiang

State Key Laboratory of Heavy Oil Processing, China University of Petroleum, Beijing 102249, China

ARTICLE INFO

Article history:
Available online 15 March 2010

Keywords:
PMMA
Three-dimensionally ordered macroporous oxides
Colloid crystal template method
Perovskite-type complex oxide
Catalysts
Soot combustion

ABSTRACT

Polymethyl methacrylate (PMMA) microspheres with diameters of 300–500 nm were prepared by using a modified emulsifier-free emulsion polymerization technique with water–oil biphase double initiators. A series of three-dimensionally ordered macroporous (3DOM) $LaCo_xFe_{1-x}O_3$ (x = 0–0.5) perovskite-type catalysts were synthesized by using colloid crystal template (CCT) method with the PMMA microspheres as template. The microspheres and 3DOM catalysts were characterized by means of XRD, FT-IR, SEM and Laser particle size analyzer, and the catalytic performances of the catalysts for diesel soot combustion were investigated by temperature-programmed oxidation (TPO) reaction. The results indicated that the obtained PMMA microspheres did not aggregate and their solid content (i.e., the mass percentage of polymer microspheres in the whole emulsion polymer) reached 9%. Their size distribution was narrow and the microspheres with different sizes can be designed under different conditions. Except $LaCo_{0.7}Fe_{0.3}O_3$, all the catalysts formed 3DOM structure and possessed a hexagonally well-ordered array. Their macroporous diameters were in the range of 250–300 nm. The 3DOM catalysts had better catalytic performances than the nonmacroporous particle catalysts for diesel soot combustion. Among the studied catalysts, the 3DOM $LaCo_{0.5}Fe_{0.5}O_3$ catalyst had the highest catalytic activity, and its T_{50} and $S^{m}_{CO_2}$ were 397 °C and 99.7%, respectively.

1. Introduction

Diesel engine vehicles are very popular owing to the relatively higher efficiency and durability of the engines compared with gasoline ones. But the emission amount of diesel soot is tens of times as much as that of gasoline ones. Soot particle is one of probable precursors to cause human carcinogen, so the emission control of diesel soot is one of the focus research topics in the field of environmental catalysis [1,2].

Perovskite-type complex metal oxides ABO_3, where A and B represent 12-coordinated and 6-coordinated metal cations, respectively, are good candidate catalysts for diesel soot combustion, because of their good redox properties, thermochemical stability and tunable catalytic performances [3]. Generally, the A position is occupied by lanthanide metals (La, Sm, etc.) and/or alkaline earth metals (Sr, Ca, Ba, etc.), and the B position is chosen from transition metals (Fe, Co, Mn, Cr, Cu, V, etc.) and noble metals. The oxidation activity of the perovskite-type catalysts can be comparable to that of the noble metal catalysts under suitable conditions. But common perovskite-type catalysts often have small specific surface area because they are prepared after high temperature calcinations [4].

In our previous work, we prepared nanometric perovskite-type catalysts to increase the specific surface area and the contact between catalyst and soot particle, and their catalytic performances for diesel soot combustion were greatly enhanced [5–7]. However, their pore diameter (<10 nm) is much smaller than the particle diameter of diesel soot (>25 nm [8]). Therefore, soot particles cannot enter the inner pores of catalysts, and only the external surface supplies the available active surface area, which leads to lower activity. Thus, it is very important to make soot easily enter the inner pores of catalysts and effectively exploit the inner pore surface for improving the catalytic activity.

The pores of 3DOM materials (pore size >50 nm) are big enough to permit diesel soot particles to enter their inner pores where the soot catalytic combustion reaction can proceed. The macropores are interconnected through windows that formed as a result of the contact between the template spheres prior to infiltration of the precursor solution. This macroporous network allows easy mass transfer of large materials as PM through the structure and less diffusional resistance to active sites, and the available active surface will be increased remarkably. Nowadays, lots of 3DOM materials were prepared successfully by CCT method with polymer microspheres as template [9–11]. But as for 3DOM perovskite-type mixed oxides, very few kinds of methods have been reported to date.

* Corresponding author.
** Corresponding author. Tel.: +86 1089731586.
E-mail addresses: liujian@cup.edu.cn (J. Liu), zhenzhao@cup.edu.cn (Z. Zhao).

0920-5861/$ – see front matter © 2010 Elsevier B.V. All rights reserved.
doi:10.1016/j.cattod.2010.01.063

Very recently, Ueda et al. [12] firstly reported 3DOM $La_{1-x}Sr_xFeO_3$ (x = 0–0.4) prepared by using an ethylene glycol (EG) solution of metal nitrate salts as precursor. In our previous work, we prepared 3DOM perovskite-type catalysts of Fe-based and Mn-based by using this method, showing better catalytic performances for diesel soot combustion than those of nanometric catalysts [13]. Hong [14] reported that the oxidizing ability follows the order of $LaCoO_3$ > $LaMnO_3$ > $LaFeO_3$, which is consistent with their activity sequence for the desired reactions, so $LaCoO_3$ has the superior activity for diesel soot combustion [15,16]. But because the melting point of the precursor containing Co cation is too low [13,17], the perovskite-type Co-based complex oxide catalysts with 3DOM structure could not be fabricated like Fe-based and Mn-based ones by this method. Before the formation of macroporous structure, the precursor has been melten. As for perovskite-type oxide catalyst, B-site cations for diesel soot combustion possess the function of catalysis, and the ion at B-site can be substituted by other ions without changing the primary crystal structure. In this way, the catalytic performances of catalysts for diesel soot combustion can be greatly enhanced. Thus, in this work, while Fe^{3+} at B-site was partially replaced by Co^{3+}, the catalysts with 3DOM structure were fabricated and the catalytic performances were improved. For comparison, the corresponding particle $LaCo_xFe_{1-x}O_3$ perovskite-type catalysts were prepared and characterized, and the effect of the particle size of the 3DOM catalysts on their catalytic performances for diesel soot combustion were also investigated.

2. Experimental section

2.1. Synthesis of PMMA microspheres

Non-crosslinked, monodisperse PMMA microspheres were synthesized using a modified emulsifier-free emulsion polymerization technique with water–oil biphase double initiators. All water in the forthcoming synthetic steps was distilled and deionized to a resistivity of at least 12 MΩ cm. Methyl methacrylate (MMA, 100 ml) was washed in a separatory funnel three times with 50 ml of 1 M NaOH, then washed three times with 50 ml of water. The washed PMMA was refined through reduced pressure distillation. A four-necked, 2000 ml round-bottomed flask was filled with the mixture of acetone (100 ml) and water (300 ml) and heated to 70 °C by a hot water bath, following the addition of the refined monomers. Attached to the flask was an electric motor driving a teflon stirring paddle, a thermometer, a condenser, and a pipet through which N_2 was bubbled to deaerate the mixture. In a separate 160 ml polyethylene bottle, 0.54 g of potassium persulfate (KPS, water-phase initiator) and 0.9 g of azodiisobutyronitrile (AIBN, oil-phase initiator) were added to 300 ml of water, then the solution was heated to 70 °C. When the water and monomers solution in the flask was heated to 70 °C, the heated initiators were added. Under constant stirring (300 r/min) and with N_2 bubbling, the mixture was kept at 70 °C for 2 h. The resulting latex microspheres were filtered through glass wool to remove any large agglomerates, then were centrifuged at 2800 r/min for 10 h to form CCT. The clear liquid was decanted and the solid block was dried in centrifugal tubes at room temperature, thus obtaining the highly ordered PMMA template. In the present studies, the average diameters of the obtained microspheres were 300–500 nm estimated by using Laser particle size analyzer. The solid content of the prepared emulsion polymer reached 9%.

2.2. Synthesis of 3DOM $LaCo_xFe_{1-x}O_3$ perovskite-type oxide catalysts

A series of 3DOM $LaCo_xFe_{1-x}O_3$ perovskite-type oxide catalysts were prepared by CCT method using ethylene glycol (EG)–methanol solution of various metal nitrates ($La(NO_3)_3{\cdot}6H_2O$, $Co(NO_3)_2{\cdot}6H_2O$, $Fe(NO_3)_3{\cdot}9H_2O$) as precursors [18]. The stoichiometric amount of mixed metal nitrates were dissolved with 15 ml of EG by stirring in a 100 ml beaker at room temperature for 2 h, and the produced solution was poured into a 50 ml volumetric flask. Methanol (6 ml) and EG were added to achieve the solution with desired concentration of methanol (the final concentration of methanol was 12 vol.%). Then the inorganic precursors were added to the CCT, permeated the voids between the close-packed spheres, and condensed into a hard inorganic framework upon drying. Excessive liquid was removed from the impregnated microspheres template via a Buchner funnel connected to vacuum. The infiltered template was allowed to dry in a desiccator using anhydrous calcium chloride at room temperature overnight. Finally, the dried sample was mixed with quartz sand (10–15 mesh) and heated in a quartz tube at the rate of 1 °C/min from room temperature to 700 °C in air for 5 h. Then EG was oxidized to the glyoxylate dianion in aqueous solution at nearly 120 °C. The metal glyoxylate converted to their metal oxide at nearly 400 °C. The perfect crystal phases were obtained by further calcination at higher temperatures (about 650 °C).

2.3. Synthesis of particle $LaCo_xFe_{1-x}O_3$ perovskite-type oxide catalysts

The particle $LaCo_xFe_{1-x}O_3$ (x = 0–0.5) perovskite-type oxide catalysts were prepared by the citric acid-ligated combustion method with various metal nitrates ($La(NO_3)_3{\cdot}6H_2O$, $Co(NO_3)_2{\cdot}6H_2O$, $Fe(NO_3)_3{\cdot}9H_2O$) as precursors. The solution was heated and evaporated to dryness with vigorous stirring, followed burning or exploding and finally the precursor was calcined at 800 °C for 4 h in static air.

2.4. Characterization of microspheres and catalysts

The structures of the microspheres and catalysts were determined by a powder X-ray diffractometer (Shimadzu XRD 6000) operating at 40 kV and 10 mA, using Cu Kα radiation (λ = 1.54184 Å) and Ni filter. The diffraction data were recorded for 2θ values from 5 to 80° with a scanning rate of 4° min^{-1}. The patterns were compared with JCPDS reference data for phase identification. The FT-IR spectra were recorded on a FTS-3000 spectrophotometer manufactured by American Digilab company. The measured wafer was prepared as a KBr pellet with the weight ratio of sample to KBr of 1/100. The resolution was set at 4 cm^{-1} during measurements. The pattern of the microspheres and catalysts were observed by SEM (FEI Quanta 200F). The average size and diameter distribution of the microspheres were determined by Laser particle size analyzer (Malern company).

2.5. Evaluation of catalytic performances of catalysts

The catalytic performances of the 3DOM and particle $LaCo_xFe_{1-x}O_3$ catalysts were evaluated with a temperature-programmed oxidation reaction (TPO) on a fixed-bed tubular quartz system. The reaction temperature was controlled through a PID-regulations system based on the measurements of a K-type thermocouple and varied during each TPO run from 200 to 600 °C at a 2 °C/min rate. The model soot, Printex-U, used in this work was provided by Degussa. Its primary particle size was 25 nm and specific surface was 100 m^2/g. The catalyst and soot were mixed at a mass ratio of 10:1 with a spatula in order to reproduce the loose contact mode, which is the most representative model of diesel particles flowing through a catalytic filter. Then the mixture placed in the tubular quartz reactor (ϕ = 10 mm) in every test. Reactant gases containing 5% O_2 and 0.2% NO balanced with Ar were

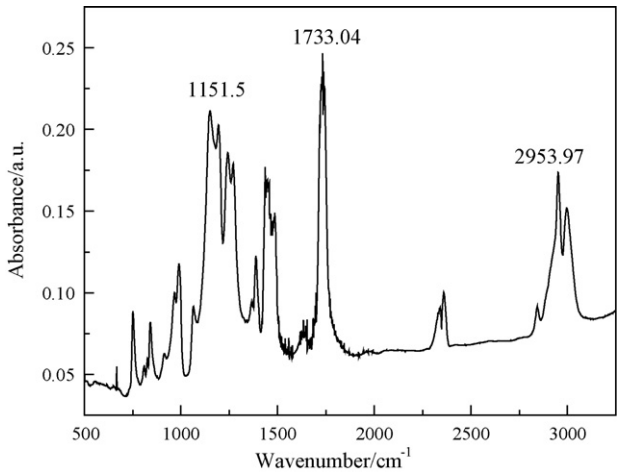

Fig. 1. The FT-IR spectrum of PMMA microspheres.

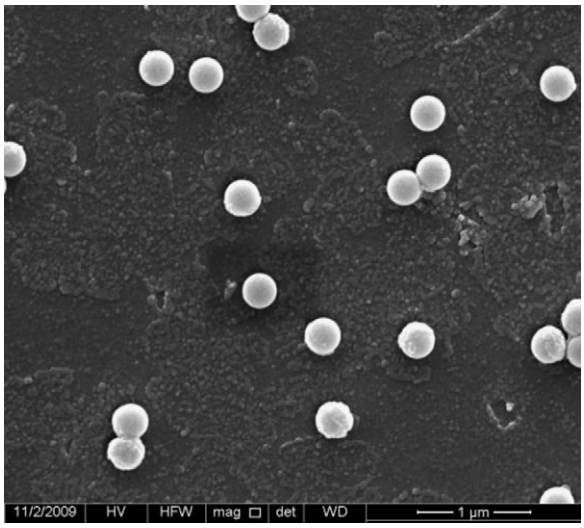

Fig. 2. The SEM image of PMMA microspheres.

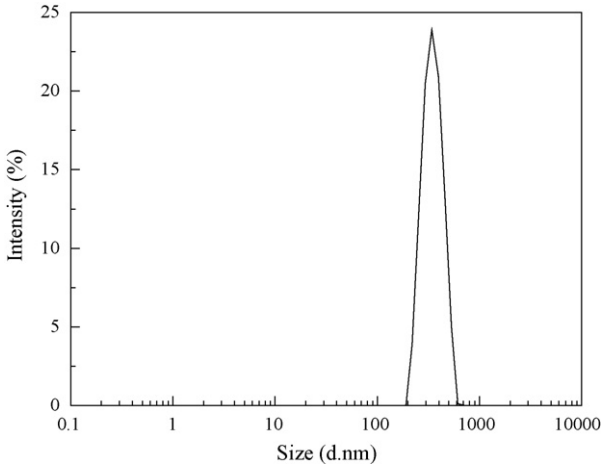

Fig. 3. The diameter distribution of PMMA spheres.

passed through a mixture of the catalyst and soot at a flow rate of 50 ml/min. The outlet gas compositions coming from the reactor were analyzed with an on-line gas chromatograph (GC, Sp-3420, Beijing) by using FID detectors. The FID was employed to determine CO and CO_2 concentrations after separating these gases over a Porapak N column and converting them to CH_4 over a Ni catalyst at 380 °C. In all TPO experiments, the reaction was not finished until the soot was completely burnt off.

3. Results and discussion

3.1. Characterization of microspheres

In the emulsifier-free emulsion polymerization system, there is no emulsifier. The particles keep stable mainly through a combination of the polymer chains, the ionic groups, or the hydrophilic groups, etc. So the surface of the obtained PMMA microspheres by this method was clean.

3.1.1. FT-IR results

Fig. 1 shows the FT-IR spectrum of PMMA microspheres. It could be seen that the sample has three strong peaks at 1152, 1733, and 2954 cm^{-1}, which corresponded to the stretching vibration of carbon oxygen single bond, the carbonyl group, and the carbon hydrogen single bond of methyl group, respectively. All these three peaks are the characteristic peaks of PMMA, indicating the presence of PMMA in the microspheres.

3.1.2. SEM and size distribution results

Fig. 2 shows the SEM image of PMMA microspheres. The particle size distribution of PMMA microspheres is presented in Fig. 3. From the images, it could be seen that the particle size distribution of the microspheres is narrow, and the average size is about 300 nm. The microspheres are uniform and spherical without any aggregation.

3.1.3. The solid content

The solid content obtained by weighing method is the mass percentage of polymer microspheres in the whole emulsion polymer. In the reaction, the solid content of reactant will increase to the maximum and then remain stable. The solid content expressed by α is given as follows:

$$\alpha = \frac{M_4 - M_1 - (M_3 - M_2) \times 0.1}{M_2 - M_1}$$

where M_1 is the initial mass of a clean weighing bottle. Adding a small amount of emulsion into it, marked the total mass as M_2. Then adding a little of inhibitor (10% ethanol solution of hydroquinone), the total mass is M_3. Finally the weighing bottle was dried at 70 °C in a vacuum drying oven until the mass maintain constant weight, which is marked as M_4.

Repeating the weighing process three times, the average value of α is the final solid content of reaction products. The solid content of obtained emulsion polymer is about 9% calculated by this method.

3.1.4. The effect of dispersion medium

Generally, the solid content of emulsion polymer is very low through emulsifier-free emulsion polymerization approach, this is probably because MMA has a lower solubility in water. One of the best approaches for solving this question is to add some dispersion medium, for instance, acetone.

Table 1 indicates that, while adding the acetone, the generated microspheres have smaller size and narrow size distribution. This is mainly because acetone can unlimitedly dissolve in water and

Table 1
Effect of dispersion medium on average particle diameter and distribution of particle diameter of microspheres.

Dispersion medium	Average size (nm)	PDI
Without acetone	484.1	0.108
With acetone	402.9	0.043

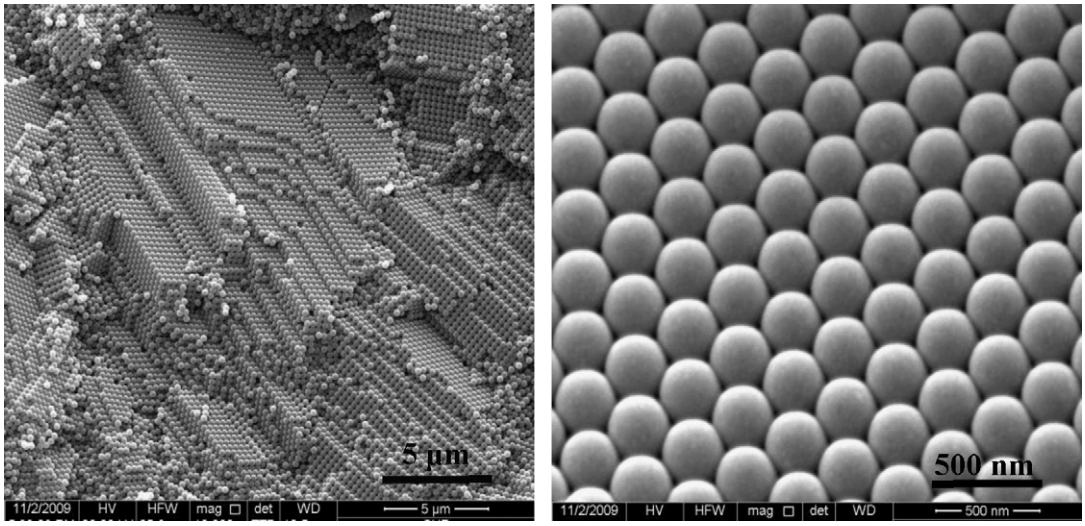

Fig. 4. The SEM images of the colloidal crystal template.

MMA, which can reduce the surface tension of water to increase the solubility of MMA. So the monomers can be dispersed into finer droplets, and their size distribution becomes narrow. Moreover, the addition of acetone can accelerate the decomposition rate of KPS, then the nucleation rate will increase. Thus, the average size of microspheres become smaller.

3.1.5. The effect of initiator

Both the water-phase initiator KPS and the oil-phase initiator AIBN were used for combining their advantages to obtain more uniform PMMA microspheres. AIBN can easily dissolve in MMA phase, while KPS can dissolve in the water-phase. At the beginning, AIBN plays a major role in the polymerization. There are still some MMA exist in water although they cannot dissolve together. So in the water-phase, the free radicals generated from the decomposition of the KPS will react with the monomers. At the step of latex particle growing, the free radicals in the water-phase increase as the KPS decomposes. Therefore, the number of the generated latex particles will become greater than that of the unreacted monomers. The free radicals begin to diffuse into the latex particles and induce polymerization to allow particles to continue growing. Moreover, induced by the KPS, the surface of the obtained microspheres would have the negative charge ($-SO_4^{2-}$), which can result in electrostatic repulsion to avoid the phenomenon of microspheres reuniting. Besides, the presence of the AIBN can reduce the polymerization time.

3.1.6. Template assembly

The microspheres synthesized by the emulsifier-free emulsion polymerization technique dispersed disorderly in the emulsion state. In order to prepare 3DOM materials, the microspheres should be assembled to a three-dimensionally ordered arrangement.

Monodisperse polymer microspheres will be orderly assembled to crystalline close-packed arrays through the particular arrangement. These arrays include the body-centered cubic (BCC), face-centered cubic (FCC) and hexagonal close-packed (HCP). FCC lattice is the most steady state in thermodynamics, even under the rapid assembly of centrifugal force. Therefore, using centrifugal method to assemble colloidal crystals can greatly shorten assembly time. In order to obtain high quality colloidal crystal template, the conditions for centrifugal assembly were investigated. The results showed that the template is more uniform under the rotational speed of 2800 r/min for 10 h.

Fig. 4 shows the SEM images of the colloidal crystal template assembled by PMMA microspheres. It can be seen that the template is uniform and orderly. Bragg diffraction will be occurred by orderly array in the visible wavelength range. A clear color change can be observed for the obtained colloidal crystal template while changing the viewing angle, which is the typical diffraction behavior of an orderly array. The appearance of Bragg diffraction phenomenon also demonstrates the good order and uniform assembly of the template.

3.2. Characterization of the catalysts

3.2.1. XRD results

The XRD patterns of the particle and 3DOM $LaCo_xFe_{1-x}O_3$ perovskite-type catalysts are shown in Fig. 5. The diffraction peaks of $LaCo_xFe_{1-x}O_3$ are in good agreement with the standard file, which corresponds to a rhombohedral system. All the characteristic diffraction peaks, which belong to $LaCo_xFe_{1-x}O_3$, are observed in the spectra of all the Fe or Co-substituted samples indicating that the obtained catalysts possessed ABO_3 perovskite-type structures with rhombohedral symmetry. Furthermore, peaks shifted to higher angle by increasing the amount of Co, indicating that the added Co metal ions incorporated into perovskite structure.

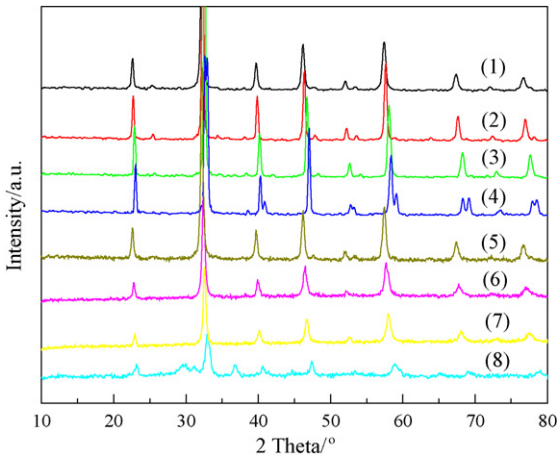

Fig. 5. The XRD patterns of $LaCo_xFe_{1-x}O_3$ perovskite-type complex oxide catalysts. (1) Particle $LaFeO_3$. (2) Particle $LaCo_{0.1}Fe_{0.9}O_3$. (3) Particle $LaCo_{0.3}Fe_{07}O_3$. (4) Particle $LaCo_{0.5}Fe_{0.5}O_3$. (5) 3DOM $LaFeO_3$. (6) 3DOM $LaCo_{0.1}Fe_{0.9}O_3$. (7) 3DOM $LaCo_{0.3}Fe_{07}O_3$. (8) 3DOM $LaCo_{0.5}Fe_{0.5}O_3$.

3.2.2. FT-IR results

BO_6 octahedron, which has A-site cation in their clearance, is the repeatable structure unit of ABO_3 crystalline structure. There are six kinds of vibrations to their IR spectra, and the stretching vibration (υ_3) is IR inactive if three pairs of B–O bonds have the same length, i.e., BO_6 octahedron having high symmetry. On the contrary, the B–O stretching vibration (υ_3) is IR active if the symmetry of BO_6 is low.

Fig. 6 shows the FT-IR spectra of the particle and 3DOM $LaCo_xFe_{1-x}O_3$ perovskite-type catalysts. There are two vibration bands, at nearly 400 and 600 cm^{-1}, in the IR spectra of all $LaCo_xFe_{1-x}O_3$ samples. The vibration band at 400 cm^{-1} belongs to the bending vibration of Fe–O or Co–O bonding in the BO_6 octahedron, and the bands at 600 cm^{-1} can be assigned to Fe–O or Co–O bond stretching vibration in the BO_6 octahedron. These results further prove that the complex oxides of $LaFe_xCo_{1-x}O_3$ possessed ABO_3 perovskite-type structures. The IR results are very consistent with those by the XRD analyses.

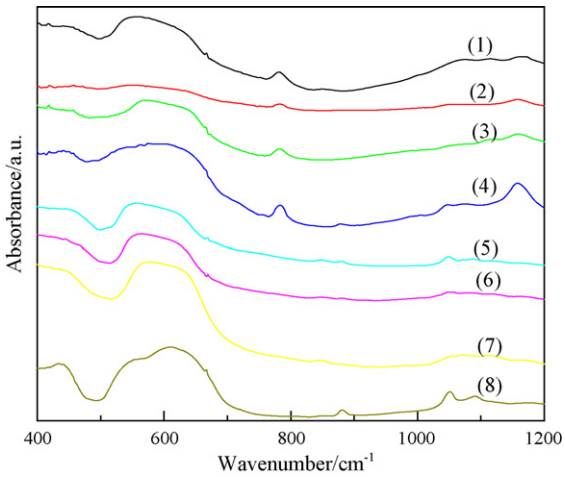

Fig. 6. The IR spectra of $LaCo_xFe_{1-x}O_3$ perovskite-type complex oxide catalysts. (1) Particle $LaFeO_3$. (2) Particle $LaCo_{0.1}Fe_{0.9}O_3$. (3) Particle $LaCo_{0.3}Fe_{07}O_3$. (4) Particle $LaCo_{0.5}Fe_{0.5}O_3$. (5) 3DOM $LaFeO_3$. (6) 3DOM $LaCo_{0.1}Fe_{0.9}O_3$. (7) 3DOM $LaCo_{0.3}Fe_{07}O_3$. (8) 3DOM $LaCo_{0.5}Fe_{0.5}O_3$.

3.2.3. SEM results

The SEM images of the 3DOM and particle $LaCo_xFe_{1-x}O_3$ catalysts are presented in Fig. 7. From the images of Fig. 7a–d, it could be seen that all the $LaCo_xFe_{1-x}O_3$ catalysts obtained by CCT method have the 3DOM structure except $LaCo_{0.7}Fe_{0.3}O_3$. The macropores

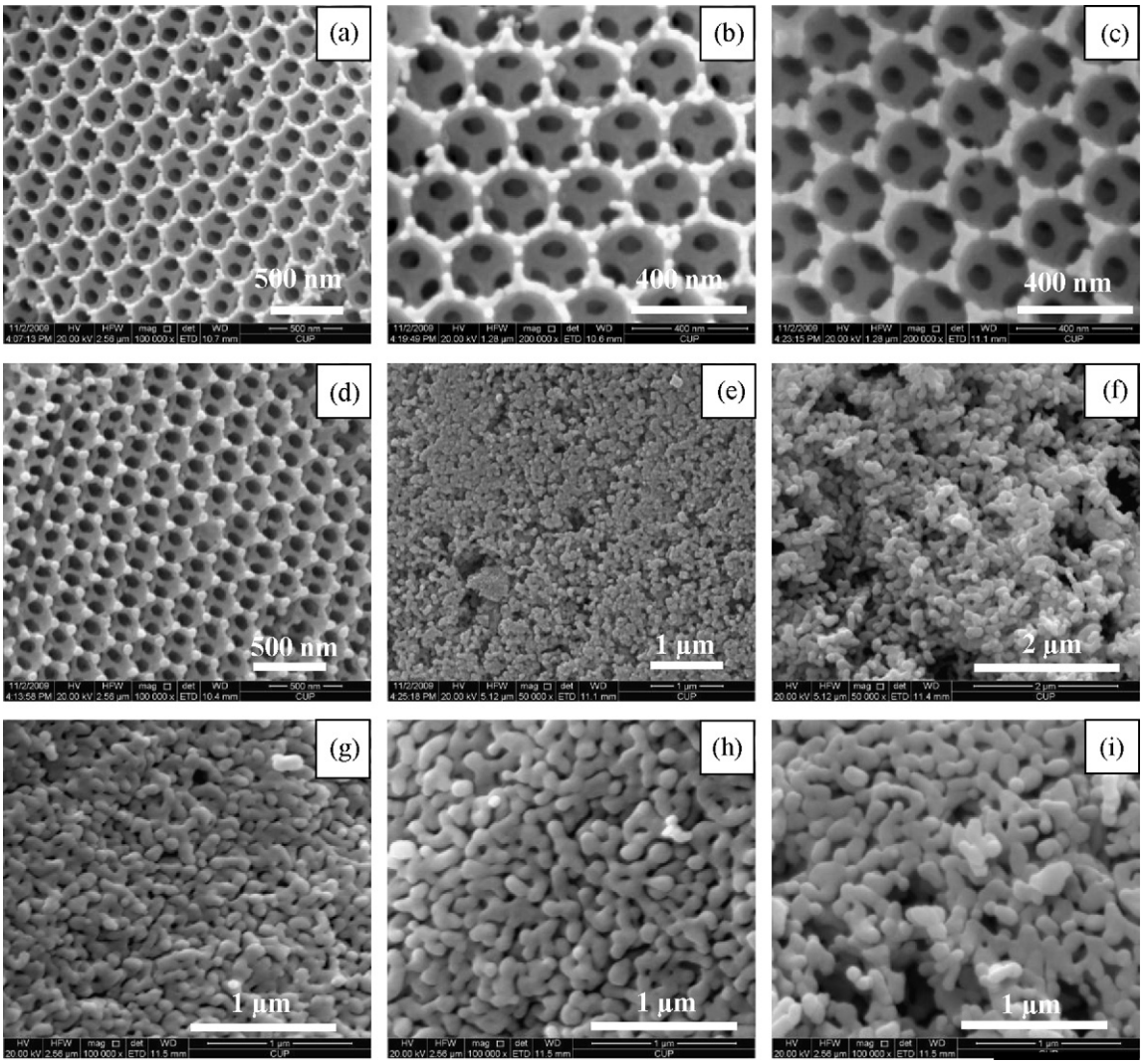

Fig. 7. The SEM images of $LaCo_xFe_{1-x}O_3$ perovskite-type complex oxide catalysts. (a) 3DOM $LaFeO_3$. (b) 3DOM-$LaCo_{0.1}Fe_{0.9}O_3$. (c) 3DOM-$LaCo_{0.3}Fe_{07}O_3$. (d) 3DOM $LaCo_{0.5}Fe_{0.5}O_3$. (e) $LaCo_{0.7}Fe_{0.3}O_3$. (f) Particle $LaFeO_3$. (g) Particle $LaCo_{0.1}Fe_{0.9}O_3$. (h) Particle $LaCo_{0.3}Fe_{07}O_3$. (i) Particle $LaCo_{0.5}Fe_{0.5}O_3$

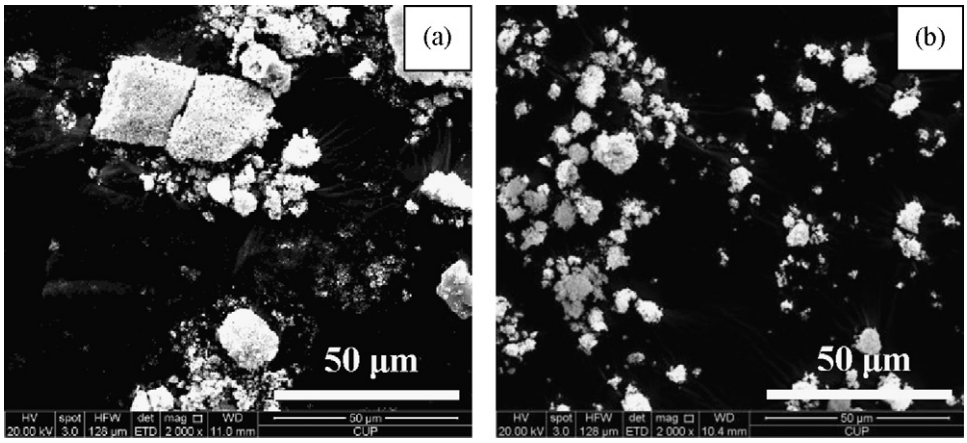

Fig. 8. The SEM images of 3DOM $LaFeO_3$ perovskite-type catalysts with different particle sizes. (a) 3DOM $LaFeO_3$ (without being grinded). (b) 3DOM $LaFeO_3$ (grinded, 5–20 μm).

are almost hemispheroidal shape and connecte with each other through the small windows. Their pore sizes estimated from the SEM image are about 250–300 nm, which corresponds to shrinkage of 15–25% compared with the initial sizes of PMMA microspheres. This shrinkage is caused by melting of the microspheres and sintering of the produced perovskite-type compound. Nevertheless, the long range orderly and uniform pore structure of the catalysts is not destroyed by this large shrinkage. The wall thickness of macroporous catalysts estimated from the SEM image is 35–45 nm. The wall seems to be composed of linearly fused grains of the produced perovskite-type compound. Three small windows in the macropore formed as a result of the contact between the template spheres could be seen. As shown in Fig. 7e, $LaCo_{0.7}Fe_{0.3}O_3$ catalyst with 3DOM structure could not be obtained by this method. It is probably because the content of Co is too high, and the melting point of the precursor containing Co cations is too low. Before the formation of macroporous structure, the precursor containing Co cations has been melten. As shown in Fig. 7f–i, the SEM images of particle $LaCo_xFe_{1-x}O_3$ perovskite-type catalysts show that the catalysts have average particle sizes in the range of 150–250 nm. The small particle sizes might lead to the higher catalytic activity for diesel soot combustion.

Fig. 8 shows the SEM photographs of 3DOM $LaFeO_3$ samples with different particle sizes. Fig. 8a shows the sample without being grinded, and Fig. 8b shows the grinded sample with the particle size of 5–20 μm. The results indicate that the particle size of the sample b is smaller than that of sample a, and its size distribution is more regular.

3.3. Catalytic performances for diesel soot combustion

The soot conversion was calculated by the integration of CO and CO_2 concentrations over the recorded time intervals. The catalytic activity was evaluated by the values of T_{10}, T_{50}, and T_{90} which were defined as the temperatures by which 10%, 50%, and 90% of the soot was oxidized, respectively, and T_{50} was the temperature of the maximum peak of CO_2 production during the TPO procedure. The selectivity to CO_2 (S_{CO_2}) was defined as the CO_2 outlet concentration (c_{CO_2}) divided by the sum of the CO_2 and CO outlet concentration, i.e., $S_{CO_2} = c_{CO_2}/(c_{CO} + c_{CO_2})$. $S^m_{CO_2}$ was denoted as S_{CO_2} at the maximum temperature at which the soot-burnt rate is the highest.

Fig. 9 shows the CO_2 concentration as a function of reaction temperature in soot combustion over the 3DOM and particle $LaCo_xFe_{1-x}O_3$ catalysts. It can be seen that the catalytic activities of the $LaCo_xFe_{1-x}O_3$ catalysts for soot combustion increase with

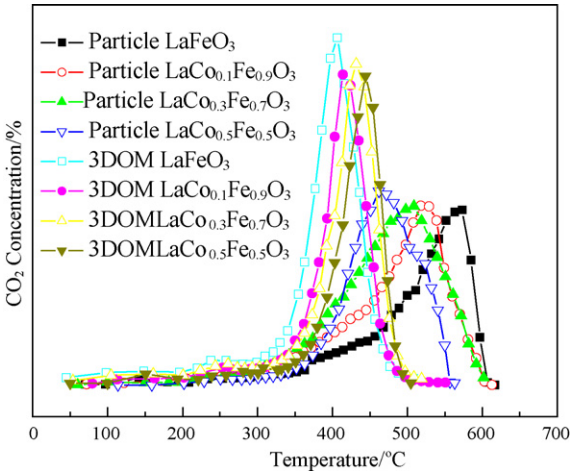

Fig. 9. The CO_2 concentration profiles for soot combustion over the catalysts.

increasing of the content of Co. The TPO experimental results of diesel soot combustion over the 3DOM and particle $LaCo_xFe_{1-x}O_3$ are listed in Table 2. For comparison, the TPO result of bare soot (i.e., without catalyst) is also included in Table 2. Its T_{50} and $S^m_{CO_2}$ are 585 °C and 65.2%, respectively. The results indicate that all the 3DOM catalysts have higher catalytic activities than the corresponding particle catalysts. Their T_{50} are decreased in the range of 70–90 °C. Moreover, the main product of soot combustion is CO_2 whose selectivity values are always above 95% for 3DOM catalysts tested. Thus, it can be concluded that the macroporous structure is superior for diesel soot combustion to the particle catalysts. Two possible reasons are considered for the enhancement of the available active surface, and thus for the enhancement of the catalytic

Table 2
The temperatures and $S^m_{CO_2}$ of soot combustion over catalysts.

Catalysts	T_{10} (°C)	T_{50} (°C)	T_{90} (°C)	$S^m_{CO_2}$ (%)
Soot (without catalyst)	482	585	646	65.2
Particle $LaFeO_3$	378	525	579	80
Particle $LaCo_{0.1}Fe_{0.9}O_3$	359	494	556	81
Particle $LaCo_{0.3}Fe_{0.7}O_3$	363	478	551	89
Particle $LaCo_{0.5}Fe_{0.5}O_3$	393	466	524	86
3DOM $LaFeO_3$	330	432	466	98.2
3DOM $LaCo_{0.1}Fe_{0.9}O_3$	282	422	462	99.7
3DOM $LaCo_{0.3}Fe_{0.7}O_3$	319	412	451	99.8
3DOM $LaCo_{0.5}Fe_{0.5}O_3$	256	397	436	99.7

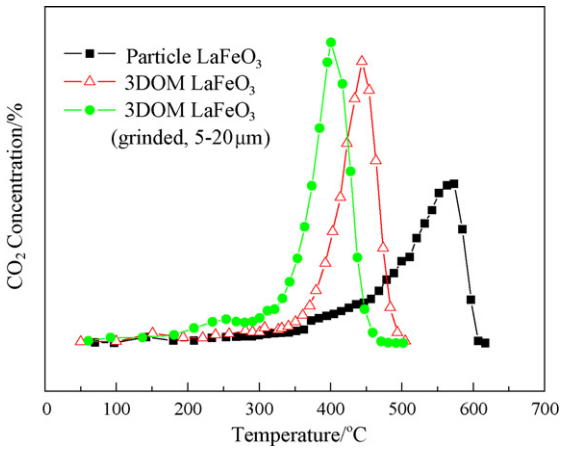

Fig. 10. The CO_2 concentration profiles for soot combustion over the 3DOM $LaFeO_3$ catalysts with different sizes.

Table 3
The temperatures and $S^m_{CO_2}$ of soot combustion over the 3DOM $LaFeO_3$ catalysts with different sizes.

Catalysts	T_{10} (°C)	T_{50} (°C)	T_{90} (°C)	$S^m_{CO_2}$ (%)
Soot (without catalyst)	482	585	646	65.2
Particle $LaFeO_3$	378	525	579	80
3DOM$LaFeO_3$ (without being grinded)	330	432	466	98.2
3DOM $LaFeO_3$ (grinded, 5–20 μm)	272	392	428	99.1

activities of the catalysts for diesel soot combustion. One is that the pore is big enough to permit diesel soot to enter their inner pores. The other one is that the uniform macroporous network allows easy mass transfer and less diffusional resistance when the large size materials such as soot particles go through the catalyst structure. The 3DOM $LaCo_{0.5}Fe_{0.5}O_3$ is the superior candidate catalyst for the catalytic combustion of soot, and its T_{10}, T_{50}, T_{90} and $S^m_{CO_2}$ are 256, 397, 436 °C, and 99.7%, respectively. Its T_{50} is decreased by 188 °C than the bare soot sample.

For comparison, the catalytic performances of the 3DOM $LaFeO_3$ samples with different particle sizes are showed in Fig. 10 and Table 3. The results indicated that the smaller is the particle size of catalysts, the better the catalytic performance is. The T_{50} of the 3DOM sample (5–20 μm) is further decreased by 40 °C compared with the sample without being grinded. It might be due to that the small particle sizes shorten the distance from the pore mouth to the site, and the diffusivity of the matter through the pore becomes easy.

4. Conclusions

(1) PMMA microspheres with diameters of 300–500 nm were prepared by using a modified emulsifier-free emulsion polymerization technique with water–oil biphase double initiators. The particle size distribution of the microspheres was narrow and the microspheres with different sizes can be designed under the different process conditions. The obtained microspheres did not show any aggregation and they were suitable for the preparation of colloidal crystal template.

(2) 3DOM $LaCo_xFe_{1-x}O_3$ (x = 0–0.5) perovskite-type complex oxide catalysts were obtained successfully by using CCT method with PMMA microspheres as template. The catalysts had a hexagonally well-ordered array and uniform pore structure as shown by SEM images, and three small windows in the macropore could be also observed. The diameters of macropores were 250–300 nm corresponding to a shrinkage ratio of 15–25%. The average thickness of its hole wall was about 35–45 nm.

(3) 3DOM $LaCo_xFe_{1-x}O_3$ catalysts had better catalytic performances for diesel soot combustion compared with the particle perovskite-type catalysts. Among the studied samples, the 3DOM $LaCo_{0.5}Fe_{0.5}O_3$ catalyst had the highest catalytic activity for soot combustion, and its T_{10}, T_{50}, T_{90} and $S^m_{CO_2}$ were 256, 397, 436 °C, and 99.7%, respectively. The particle size also had a large effect on the catalytic performances of studied catalysts for diesel soot combustion. The T_{50} temperature of the grinded 3DOM $LaFeO_3$ with the relatively small particle size of 5–20 μm was further reduced to 392 °C, and $S^m_{CO_2}$ increased to 99.1%.

Acknowledgements

This work was supported by the National Natural Science Foundation of China (Nos. 20803093 and 20833011), the Doctor Select Foundation for the University of State Education Ministry (No. 200804251016), the Beijing Outstanding Ph.D. Thesis Foundation (No. YB 20091141401), and 863 Program (No. SQ2009AA06Z3488052).

References

[1] C.A. Querini, L.M. Cornaglia, M.A. Ulla, E.E. Miro, Appl. Catal. B 20 (1999) 165.
[2] H. He, D. Weng, L.Y. Zi, Environ. Sci. 28 (2007) 1169.
[3] Y. Teraoka, K. Kanada, S. Kagawa, Appl. Catal. B 34 (2001) 73.
[4] H. Tanaka, M. Misono, Curr. Opin. Solid State Mater. 5 (2001) 381.
[5] H. Wang, Z. Zhao, P. Liang, C.M. Xu, A.J. Duan, G.Y. Jiang, J. Xu, J. Liu, Catal. Lett. 124 (2008) 91.
[6] H. Wang, Z. Zhao, C.M. Xu, J. Liu, Catal. Lett. 102 (2005) 251.
[7] J. Liu, Z. Zhao, J. Lan, C.M. Xu, A.J. Duan, G.Y. Jiang, X.P. Wang, H. He, J. Phys. Chem. C 113 (2009) 17114.
[8] B.R. Stanmore, J.F. Brilhac, P. Gilot, Carbon 39 (2001) 2247.
[9] S.W. Woo, K. Dokko, K. Kanamura, Electrochim. Acta 53 (2007) 79.
[10] E.O. Chi, Y.N. Kim, J.Ch. Kim, N.H. Hur, Chem. Mater. 15 (2003) 1929.
[11] G.Z. Zhang, Z. Zhao, J. Liu, G.Y. Jiang, A.J. Duan, J.X. Zheng, S.L. Chen, R.X. Zhou, Chem. Commun. 46 (2010) 457.
[12] M. Sadakane, T. Asanuma, J. Kubo, W. Ueda, Chem. Mater. 17 (2005) 3546.
[13] G.Z. Zhang, Ph D Thesis, China University of Petroleum, Beijing, 2009.
[14] S.S. Hong, G.D. Lee, Catal. Today 63 (2000) 397.
[15] H. Wang, Z. Zhao, C.M. Xu, A.J. Duan, J. Liu, Y.L. Chi, Chin. J. Catal. 29 (2008) 649.
[16] J. Liu, Z. Zhao, C.M. Xu, H. Wang, React. Kinet. Catal. L 87 (2006) 107.
[17] J. Liu, Z. Zhao, J.Q. Wang, C.M. Xu, A.J. Duan, G.Y. Jiang, Q. Yang, Appl. Catal. B 84 (2008) 185.
[18] M. Sadakane, T. Asanuma, N. Kato, C. Takahashi, W. Ueda, Chem. Mater. 19 (2007) 5779.